Supporting Information

Copper Rhodium Nanosheets Alloy for Electrochemical NO Reduction Reaction via the Selective Intermediate Adsorption

Yechuan Zhang,[a] Jiachen Zhang,[a] Fang Peng,[a]* Huajun Yang,[a] Zhengxiang Gu,[a]* Hanjun Sun[a]*

[a] *Jiangsu Key Laboratory of New Power Batteries, Jiangsu Collaborative Innovation Centre of Biomedical Functional Materials, School of Chemistry and Materials Science, Nanjing Normal University, Nanjing 210023, China.*

** Corresponding Author.*

Supplementary Text

1. Experimental section

1.1 Chemicals and materials.

$Rh(acac)_3$ (>99%), $Cu(acac)_2$ (>99.0%), $Rh_3(CO)_{12}$, copper acetylacetonate (≥99.99%), tri-n-octylphosphine oxide (>99.0%), Ruthenium(III) chloride hydrate (RuCl3·xH2O, 35.0-42.0% Ru basis), Ru(III) acetylacetonate ($Ru(acac)_3$, 99%), oleylamine (OAm, 80%-90%), benzyl alcohol (99%), D-(+)-glucose (99%), n-octanol (99%), salicylic acid (AR, 99.5%), sodium hydroxide (NaOH, AR, 96%), trisodium citrate dihydrate (98%), sodium nitrate ($NaNO_3$, 99%), sodium nitrite ($NaNO_2$, 99.99% metals basis), ammonium chloride (NH_4Cl, ACS, 99.5%), sodium sulfate anhydrous (Na_2SO_4, 99%), Zinc acetate ($Zn(Ac)_2$, AR, 99.0%), N-(1-naphthyl)ethylenediamine dihydrochloride (AR, 98%), p-aminobenzenesulfonamide (AR, ≥ 99%), phosphoric acid (H_3PO_4, ACS, ≥ 85 wt.% in H_2O, ρ = 1.70 g/mL), sodium nitrate- ^{15}N (99 atom%, ≥ 98.5%), ammonium chloride- ^{15}N (98 atom%, ≥ 98%) and maleic acid (AR, ≥ 99.0% (HPLC)) were supplied by purchased from Shanghai Aladdin Biochemical Technology Co., Ltd. Dimethyl sulfoxide-d_6 (DMSO-d_6), and Nafion 115 membrane were purchased from Aladdin Chemistry Co., Ltd (Shanghai, China). Deionized (DI) water was produced using a Millipore Milli-Q grade, with a resistivity of 18.2 MΩ cm. All chemicals were used without any further purification.

1.2 Electrochemical measurements.

Electrocatalytic NORR measurements were conducted in a NO-saturated 0.1 M Na_2SO_4 solution using a gas-tight H-type cell separated by a Nafion 115 membrane at room temperature. Electrochemical measurements were performed on a CHI-660E electrochemical workstation in a three-electrode configuration including a working electrode prepared from the catalyst (CC, 1 × 1 cm^2), a reference electrode (Ag/AgCl), and a counter electrode prepared from graphite rods. The self-supporting array grown on the carbon cloth (1×1 cm, mass loading ~ 1.25 mg/cm^2) was directly used as a working electrode. The measured potentials via the Hg/HgO electrode were converted to those based on a reversible hydrogen electrode (RHE) by the Nernst equation:

E (V. vs RHE) = E (V. vs Ag/AgCl) + 0.0591*pH + 0.198 V. (1)

Prior to the NORR test, the feeding gases were purified through two glass bubblers containing a 4 M KOH solution and the cathodic compartment was purged with Ar for at least 30 min to remove residual oxygen. The linear sweep voltammetry curves were established at a scanning rate of 5 mV/s before 50 cycles of the cyclic voltammetry tests were performed at a scan rate of 50 mV/s to obtain stable curves. The chronoamperometry was used to evaluate the stability under different current densities. Electrochemical impedance spectroscopy (EIS) measurements were performed over a frequency range of 0.1-1.0 x 10^6 Hz by applying an AC amplitude of 50 mV. All data were within 90% of iR-correction.

1.3 Preparation of the working electrode.

2.5 mg of the catalyst was dispersed in 2 mL of ethanol by sonication for 30 min. 40 μL of a Nafion solution was added to the catalyst solution and the mixture was sonicated for 30 min to obtain a uniform ink. The ink was loaded onto a carbon paper with an area of 1×1 cm^{-2}. The mass loading was calculated to be 1.25 mg cm^{-2}. The area of the working electrode used in the electrochemical test was 1×1 cm^2.

1.4 Calculation of FE and the NH_3 yield rate.

The FE for NH_3 electrosynthesis was defined as the amount of electric charge used for producing NH_3 divided by the total charge passed through the electrodes during electrolysis. The FE was calculated according to the following equation:

$$FE = n \times F \times c \times V / (M \times Q)\ (S1) \quad (2)$$

The NH_3 yield was calculated using the following equation:

$$NH_3\ yield = C_{NH3} \times V / (17 \times t \times S)\ (S2) \quad (3)$$

Where n is the number of electrons needed to produce one product molecule, F is the Faraday constant (96485 C mol^{-1}); C is the measured mass concentration of the product; V is the volume of the cathodic reaction electrolyte (50 mL); M is the relative molecular mass of a specific product; Q is the quantity of applied charge/electricity; t is the duration for applying the potential (1 h); and S is the geometric area of the working electrode (1 cm^2).

2. Supplementary results.

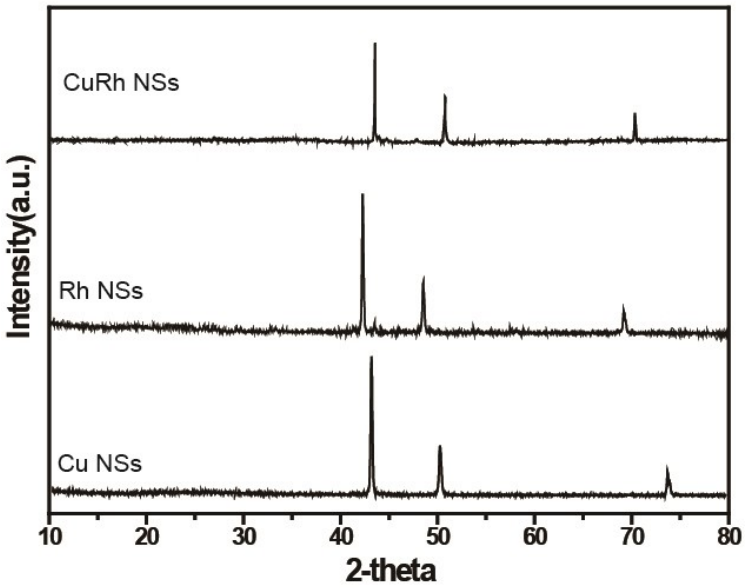

Figure S1. XRD patterns of CuRh NSs, Rh NSs, and Cu NSs.

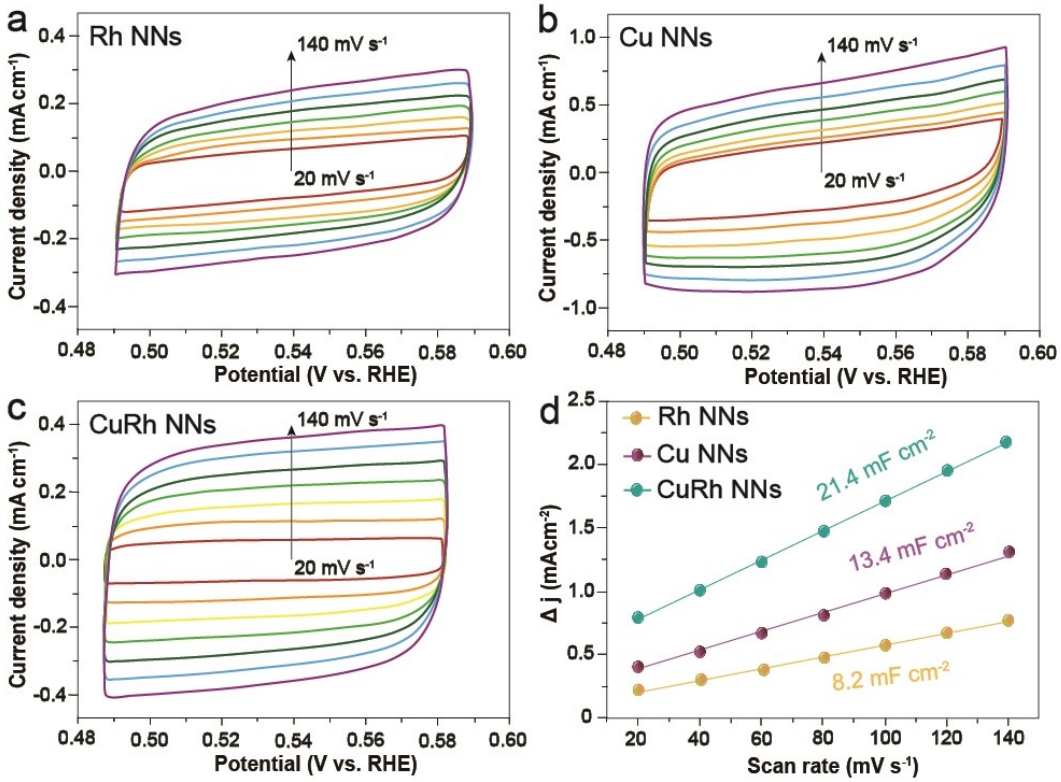

Figure S2. CV curves of (a) Rh NSs, (b) Cu NSs, and (c) CuRh NSs at scan rates from 10 to 100 mV s^{-1}. (d) ECSA results of Rh NSs, and Cu NSs, CuRh NSs.

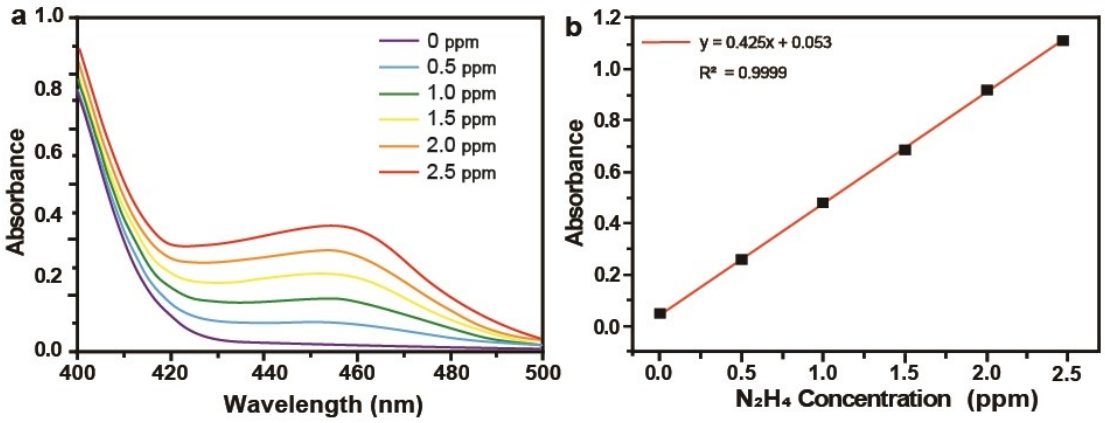

Figure S3. (a) UV−vis absorption spectra for N_2H_4–N at various concentrations. (b) A calibration curve for estimating the concentrations of N_2H_4–N.

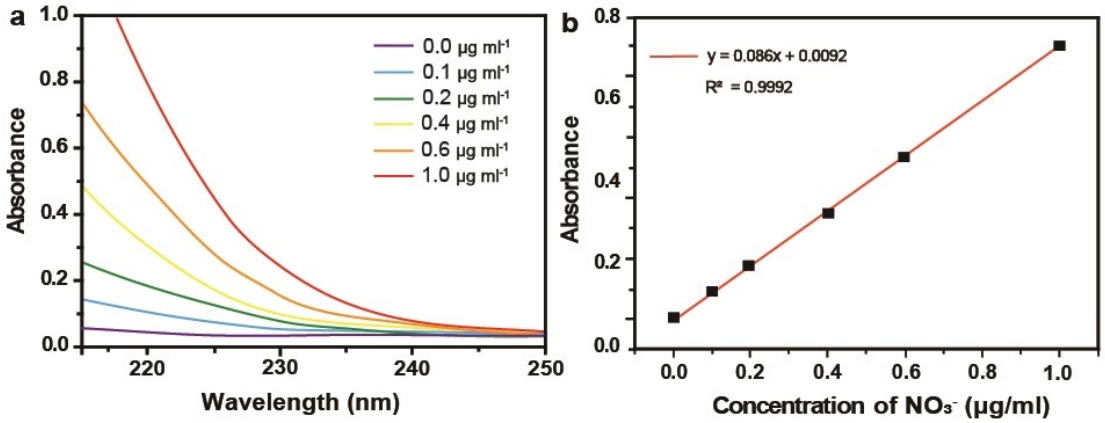

Figure S4. (a) UV−vis absorption spectra for NO_3^-–N at various concentrations. (b) A calibration curve for estimating the concentrations of NO_3^-–N.

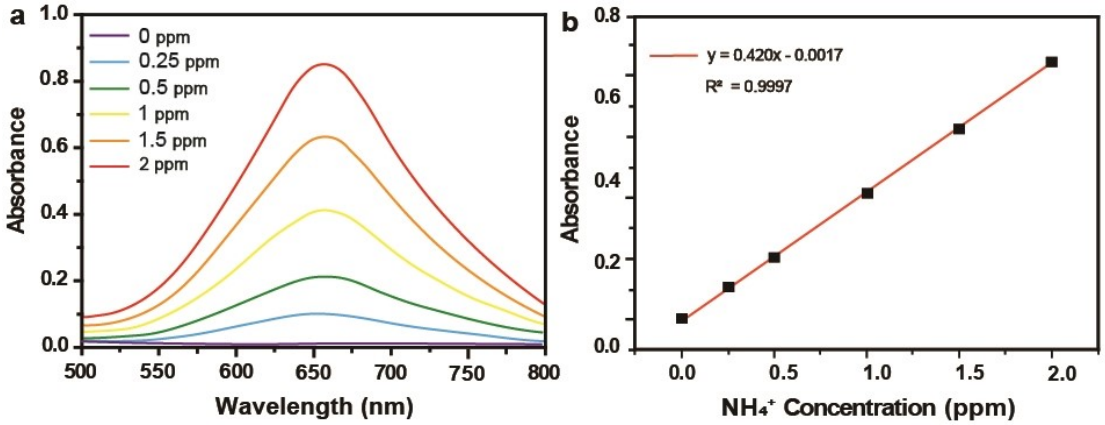

Figure S5. (a) UV−vis absorption spectra for NH_3–N at various concentrations. (b) A calibration curve for estimating the concentrations of NH_3–N.

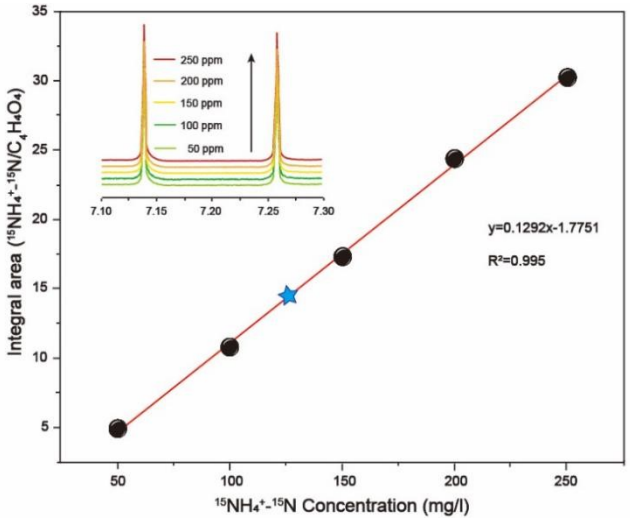

Figure S6. The standard curve of the integral area ($^{15}NH_4^+$-N/$C_4H_4O_4$) against the $^{15}NH_4^+$-N concentration.

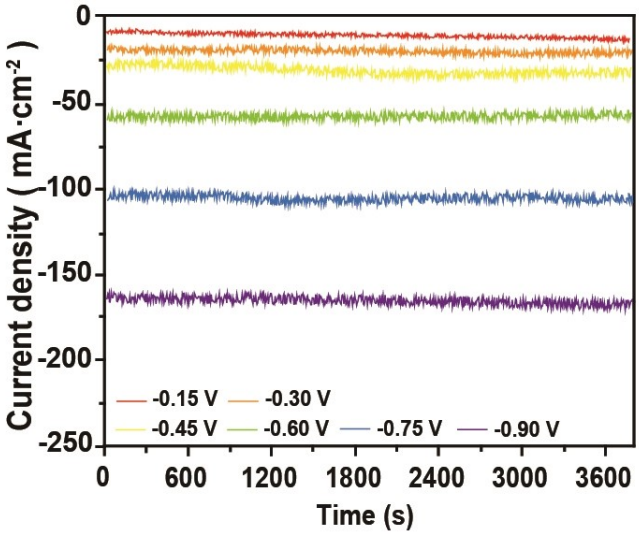

Figure S7. Chronoamperometric recordings of constant potential NH_3 synthesis performance of CuRh NSs at a series of potentials.

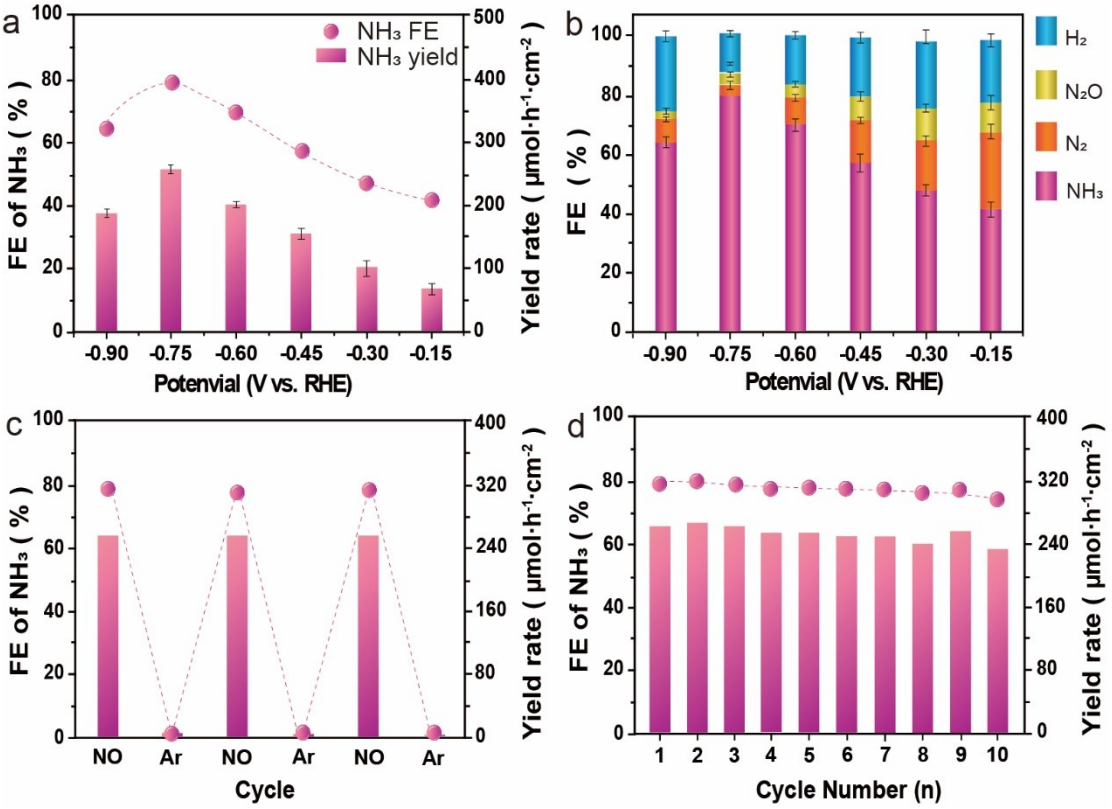

Figure S8. NH_3 synthesis performance of Cu NSs at a series of potentials. (a) NH_3 yield rates and FE_{NH3}. (b) Faradaic efficiencies of NORR products at different potentials from −0.15 V to −0.90 V vs RHE. (c) FE_{NH3} for NO-Ar switching cycles on Cu NSs at −0.60 V. (d) FE_{NH3} of 10 cycles on Cu NSs at −0.60 V.

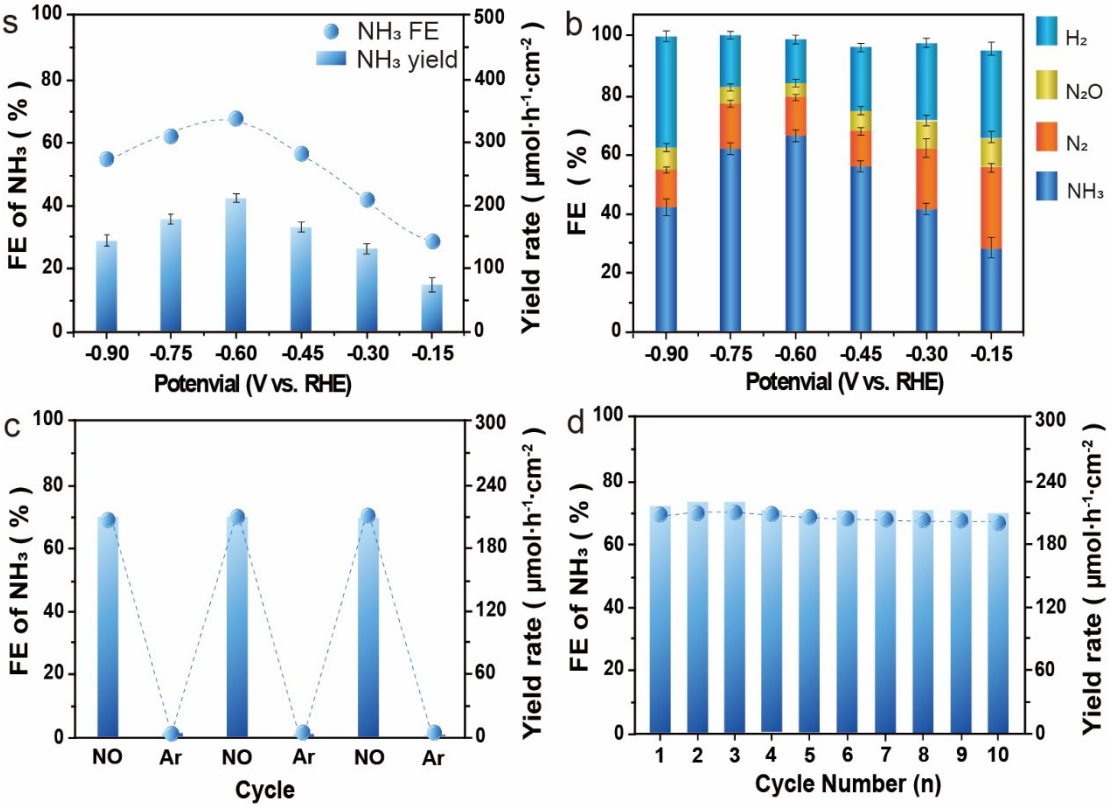

Figure S9. NH_3 synthesis performance of Rh NSs at a series of potentials. (a) NH_3 yield rates and FE_{NH3}. (b) Faradaic efficiencies of NORR products at different potentials from −0.15 V to −0.90 V vs RHE. (c) FE_{NH3} for NO-Ar switching cycles on Rh NSs at −0.60 V. (d) FE_{NH3} for 10 cycles on Rh NSs at −0.60 V.

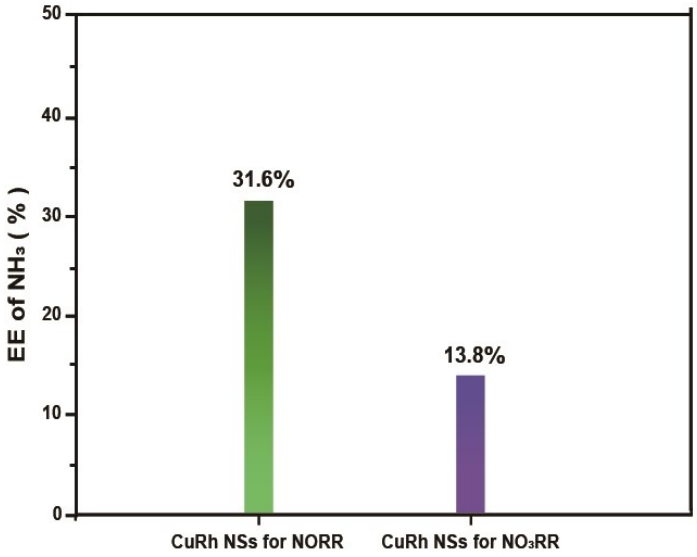

Figure S10. The EE of NH_3 for NORR and NO_3RR using CuRh nanosheets.

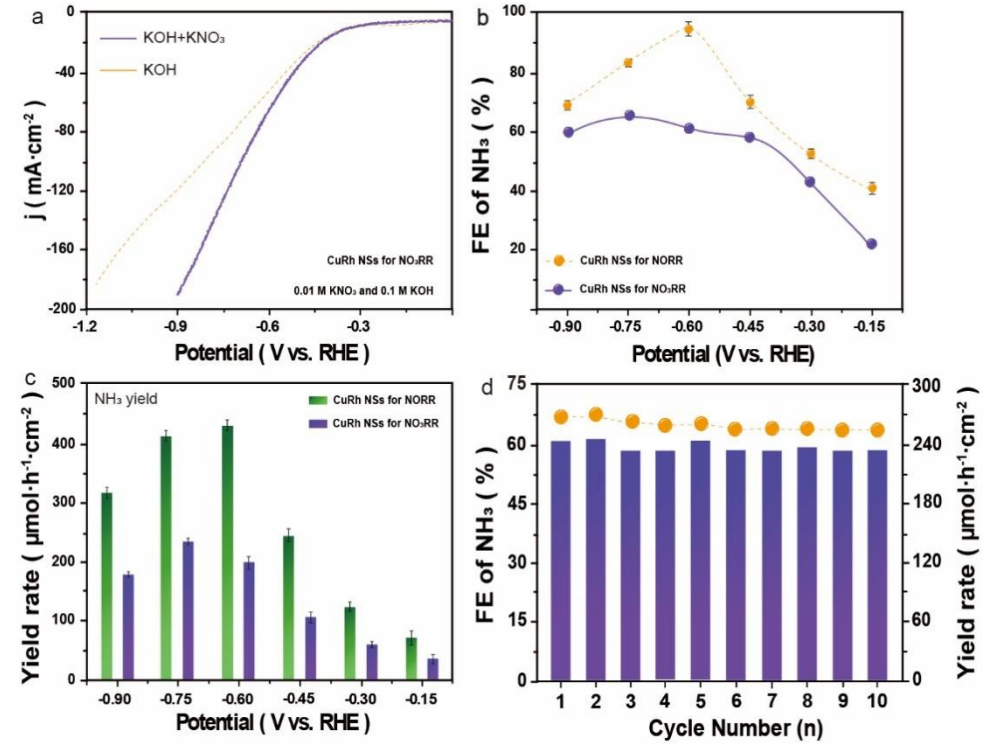

Figure S11. CuRh NSs catalytic performance of NO_3RR. (a) LSV at a scan rate of 5 mV s^{-1}. (b) Faradaic Efficiency of using CuRh NSs for NORR (purple solid line with dots) and NO_3RR (yellow dash line with dots). (c) NH_3 yield rate of NORR and NO_3RR based on CuRh NSs. (d) Cycling tests of the CuRh NSs for the reduction process at −0.60 V regarding the yield rate and FE of NH_3.

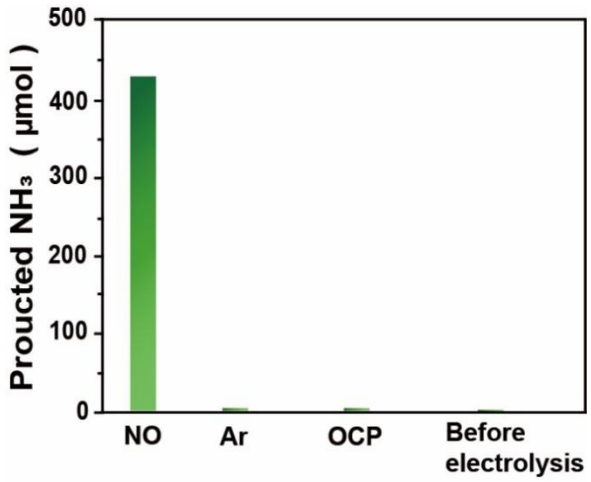

Figure S12. The amount of produced NH_3 under different conditions: (1) before electrolysis; (2) electrolysis on CuRh NSs in an Ar-saturated electrolyte at –0.6 V; (3) electrolysis on CuRh NSs in a NO-saturated electrolyte at an open-circuit potential; (4) electrolysis on CuRh NSs in a NO-saturated electrolyte at –0.6 V.

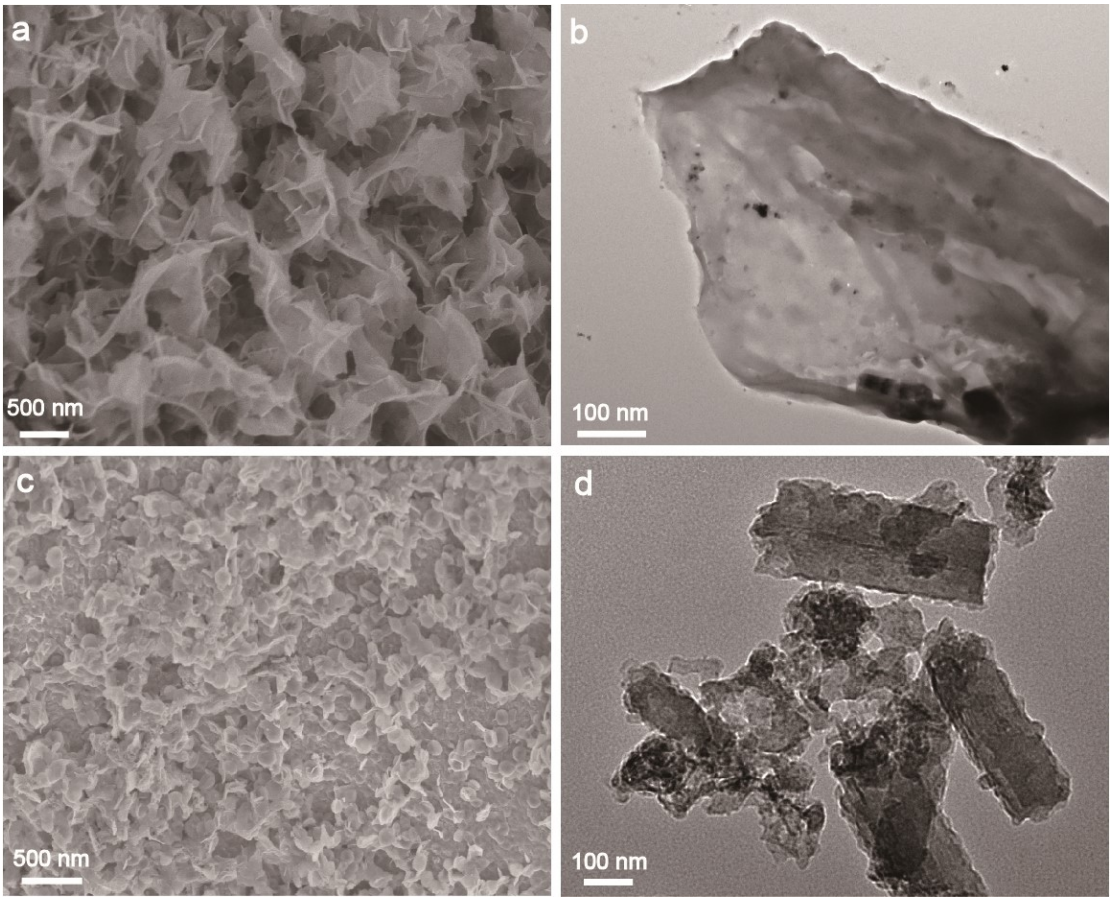

Figure S13. SEM (a) and TEM (b) images of CuRh NSs after 85-h catalytic test. (c) SEM and (d) TEM images of CuRh NSs after a 170-h test.

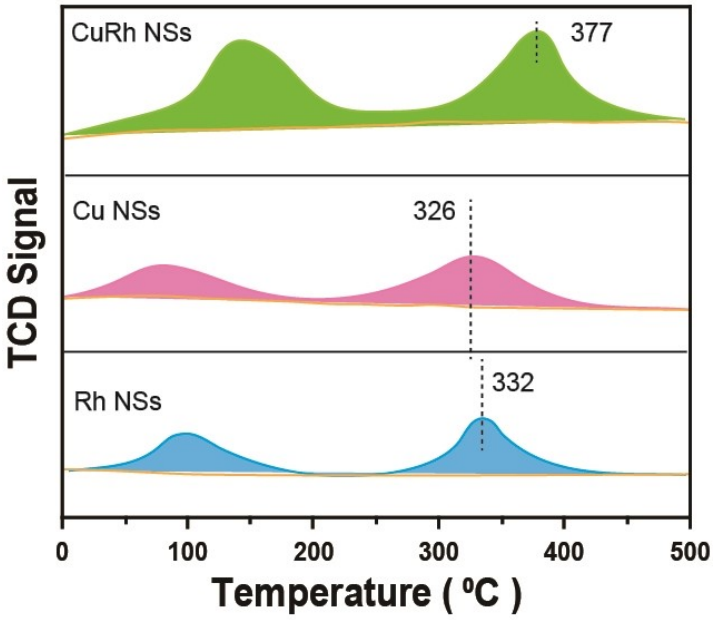

Figure S14. NO-TPD profiles of the CuRh nanosheets, Cu nanosheets, and Rh nanosheets.

Table S1. Electrocatalytic NO reduction performances at an ambient condition by the CuRh NSs in this study and recently reported catalysts.

Catalysts	Electrolyte	Ammonia yield rate (μmol h^{-1} cm^{-2})	FE_{NH3} (%)	Reference
CuRh NSs	**0.1 M Na_2SO_4**	**436.0**	**93.1**	**This study**
Cu_2O	0.1 M HCl	94.1	75.05	S1
NiO	0.1 M Na_2SO_4	125.3	90.0	S2
a-$B_{2.6}C$@TiO_2/Ti	0.1 M Na_2SO_4	216.4	87.6	S3
Cu_1/MoS_2	0.5 M Na_2SO_4	337.5	90.6	S4
Fe_1/MoS_{2-x}	0.5 M Na_2SO_4	288.2	82.5	S5
Mo_2C	0.5 M Na_2SO_4	122.7	86.3	S6
NiFe-LDHC	0.25 M Li_2SO_4	112	82	S7
Nb_1BNC	1 M HCl	295.2	77.0 ± 0.6%	S8
W_1/MoO_{3-x}	0.5 M Na_2SO_4	308.6	91.2	S9

References:

S1 C. Bai, S. Fan, X. Li, Z. Niu, J. Wang, Z. Liu, D. Zhang, *Adv. Funct. Mater.* **2022**, *32*, 2205569.

S2. P. Liu, J. Liang, J. Wang, L. Zhang, J. Li, L. Yue, Y. Ren, T. Li, Y. Luo, N. Li, B. Tang, Q. Liu, A. M. Asiri, Q. Kong, X. Sun, *Chem. Commun.* **2021**, *57*, 13562-13565.

S3. J. Liang, P. Liu, Q. Li, T. Li, L. Yue, Y. Luo, Q. Li, N. Li, B. Tang, A. A. Alshehri, I. Shakir, P. O. Agboola, C. Sun, X. Sun, *Angew. Chem. Int. Ed.* **2022**, *61*, e202202087.

S4. G. Meng, T. Wei, W. Liu, W. Li, S. Zhang, W. Liu, Q. Liu, H. Bao, J. Luo, X. Liu, *Chem. Commun.* **2022**, *58*, 8097.

S5. D. Wang, Z.-W. Chen, K. Gu, C. Chen, Y. Liu, W. X, C. V. Singh, S. Wang, *J. Am. Chem. Soc.* **2023**, *145*, 6899.

S6. H. Zhang, Y. Li, C. Cheng, J. Zhou, P. Yin, H. Wu, Z. Liang, J. Zhang, Q. Yun, A. L. Wang, *Angew. Chem. Int. Ed.* **2022**, *62*, e2022133.

S7. S. Zhao, J. Liu, Z. Zhang, C. Zhu, G. Shi, J. Wu, C. Yang, Q. Wang, M. Chang, K. Liu, S. Li, *Chem.* **2023**, *8,* 1281.

S8. X. Peng, Y. Mi, H. Bao, Y. Liu, D. Qi, Y. Qiu, L. Zhuo, S. Zhao, J. Sun, X. Tang, J. Luo, X. Liu, *Nano Energy*, 2020, 78, 105321.

S9. K. Chen, J. Wang, H. Zhang, D. Ma, K. Chu, *Nano. Lett.* **2023**, 23, 1735-1742.